

# Thermoreflectance of metal transducers for optical pump-probe studies of thermal properties

R. B. Wilson,\* Brent A. Apgar, Lane W. Martin, and David G. Cahill

Department of Materials Science, and Materials Research Laboratory, University of Illinois, Urbana, Illinois 61801, USA

\*wilson81@illinois.edu

**Abstract:** We report measurements of the temperature dependence of the optical reflectivity,  $dR/dT$  of fifteen metallic elements at a wavelength of  $\lambda = 1.03 \mu\text{m}$  by time-domain thermoreflectance (TDTR); and the thermoreflectance of thin-films of Pt, Ta, Al, Au, SrRuO<sub>3</sub>, and LaNiO<sub>3</sub> over the wavelength range  $0.4 < \lambda < 1.6 \mu\text{m}$  using variable angle spectroscopic ellipsometry. At  $\lambda = 1.03 \mu\text{m}$ , Al, Ta, Re, Ru, have high values of thermoreflectance,  $dR/dT > 6 \cdot 10^{-5} \text{ K}^{-1}$ , and are good choices as optical transducers for TDTR experiments using a Yb: fiber laser oscillator. If low optical reflectivity and the associated high degree of steady-state heating are not a concern, LaNiO<sub>3</sub> provides an exceptionally sensitive thermometer in the infrared;  $(1/R)(dR/dT) > 2.5 \cdot 10^{-4} \text{ K}^{-1}$  in the wavelength range  $0.85 < \lambda < 1.3 \mu\text{m}$ . This compilation of data will assist in the design and interpretation of optical pump-probe studies of thermal properties.

©2012 Optical Society of America

**OCIS codes:** (320.7100) Ultrafast measurements; (110.6820) Thermal imaging; (160.3900) Metals; (350.5340) Photothermal effects.

---

## References and links

1. D. G. Cahill, "Analysis of heat flow in layered structures for time-domain thermoreflectance," *Rev. Sci. Instrum.* **75**(12), 5119–5122 (2004).
2. A. J. Schmidt, R. Cheaito, and M. Chiesa, "A frequency-domain thermoreflectance method for the characterization of thermal properties," *Rev. Sci. Instrum.* **80**(9), 094901–094906 (2009).
3. J. A. Malen, K. Baheti, T. Tong, Y. Zhao, J. A. Hudgings, and A. Majumdar, "Optical measurement of thermal conductivity using fiber aligned frequency domain thermoreflectance," *J. Heat Transfer* **133**(8), 081601 (2011).
4. Y. K. Koh, Y. Cao, D. G. Cahill, and D. Jena, "Heat-transport mechanisms in superlattices," *Adv. Funct. Mater.* **19**(4), 610–615 (2009).
5. C. Chiritescu, D. G. Cahill, N. Nguyen, D. Johnson, A. Bodapati, P. Koblinski, and P. Zschack, "Ultralow thermal conductivity in disordered, layered WSe<sub>2</sub> crystals," *Science* **315**(5810), 351–353 (2007).
6. Y. K. Koh and D. G. Cahill, "Frequency dependence of the thermal conductivity of semiconductor alloys," *Phys. Rev. B* **76**(7), 075207 (2007).
7. A. J. Minnich, J. A. Johnson, A. J. Schmidt, K. Esfarjani, M. S. Dresselhaus, K. A. Nelson, and G. Chen, "Thermal conductivity spectroscopy technique to measure phonon mean free paths," *Phys. Rev. Lett.* **107**(9), 095901 (2011).
8. E. Colavita, A. Franciosi, C. Mariani, and R. Rosei, "Thermoreflectance test of W, Mo, and paramagnetic Cr band structures," *Phys. Rev. B* **27**(8), 4684–4693 (1983).
9. R. Rosei and D. W. Lynch, "Thermomodulation Spectra of Al, Au, and Cu," *Phys. Rev. B* **5**(10), 3883–3894 (1972).
10. R. Rosei, E. Colavita, A. Franciosi, J. H. Weaver, and D. T. Peterson, "Electronic structure of the bcc transition metals: thermoreflectance studies of bulk V, Nb, Ta, and  $\alpha\text{TaHx}$ ," *Phys. Rev. B* **21**(8), 3152–3157 (1980).
11. W. J. Scouler, "Temperature-modulated reflectance of gold from 2 to 10 eV," *Phys. Rev. Lett.* **18**(12), 445–448 (1967).
12. Y. Wang, J. Y. Park, Y. K. Koh, and D. G. Cahill, "Thermoreflectance of metal transducers for time-domain thermoreflectance," *J. Appl. Phys.* **108**(4), 043507 (2010).
13. G. Tessier, S. Hole, and D. Fournier, "Quantitative thermal imaging by synchronous thermoreflectance with optimized illumination wavelengths," *Appl. Phys. Lett.* **78**(16), 2267–2269 (2001).

14. M. Otter, "Temperaturabhängigkeit der optischen konstanten massiver metalle," *Zeitschrift für Physik A Hadrons and Nuclei* **161**, 539–549 (1961).
15. W.-P. Hsieh and D. G. Cahill, "Ta and Au(Pd) alloy metal film transducers for time-domain thermoreflectance at high pressures," *J. Appl. Phys.* **109**(11), 113520 (2011).
16. J. Alper and K. Hamad-Schifferli, "Effect of ligands on thermal dissipation from gold nanorods," *Langmuir* **26**(6), 3786–3789 (2010).
17. X. Huang, S. Neretina, and M. A. El-Sayed, "Gold nanorods: from synthesis and properties to biological and biomedical applications," *Adv. Mater. (Deerfield Beach Fla.)* **21**(48), 4880–4910 (2009).
18. S. Sato, "Nucleation properties of magnetron-sputtered tantalum," *Thin Solid Films* **94**(4), 321–329 (1982).
19. K. Kang, Y. K. Koh, C. Chiritescu, X. Zheng, and D. G. Cahill, "Two-tint pump-probe measurements using a femtosecond laser oscillator and sharp-edged optical filters," *Rev. Sci. Instrum.* **79**(11), 114901 (2008).
20. J. A. McCaulley, V. M. Donnelly, M. Vernon, and I. Taha, "Temperature dependence of the near-infrared refractive index of silicon, gallium arsenide, and indium phosphide," *Phys. Rev. B Condens. Matter* **49**(11), 7408–7417 (1994).
21. Y. S. Touloukian, ed., *Thermophysical Properties of Matter: Volume 14* (IFI/Plenum, 1979).
22. J. H. Weaver and H. P. R. Frederikse, *CRC Handbook of Chemistry and Physics* (CRC Press, 1977)
23. P. B. Johnson and R. W. Christy, "Optical constants of the noble metals," *Phys. Rev. B* **6**(12), 4370–4379 (1972).
24. B. Berini, W. Noun, Y. Dumont, E. Popova, and N. Keller, "High temperature ellipsometry of the conductive oxide LaNiO<sub>3</sub>," *J. Appl. Phys.* **101**(2), 023527–023529 (2007).
25. J. M. Ziman, *Electrons and Phonons* (Oxford University Press, 1960)

## 1. Introduction

Time-domain thermoreflectance [1] (TDTR) and frequency-domain thermoreflectance [2, 3] (FDTR) are optical-pump-probe techniques for studying heat flow on ultrafast time scales and nanoscale length scales. TDTR and FDTR monitor the evolution of the surface temperature of a thin-metal-film in the time and frequency domain. The flexibility of these techniques has enabled experimental studies of thermal transport in a diverse set of systems for a wide variety of applications. For example, these techniques have enabled the characterization of nanostructured semiconductors for thermoelectric applications [4], the discovery of ultralow thermal conductivity materials [5], and investigations of phonon mean-free-paths and quasi-ballistic-phonon-transport in dielectrics [6, 7].

The optical transducer is a critical consideration in the design of a TDTR or FDTR experiment. Physical and chemical properties of the transducer such as susceptibility to oxidation and corrosion, stability at high temperatures, thermal conductivity, specific heat, and adhesion to substrates can all be important factors. The process of choosing the best transducer for a particular experiment is complicated by the fact that the temperature dependence of the optical properties of most materials are not readily available in the literature. In TDTR and FDTR measurements, the signal strength depends on the product of the optical absorbance of the metal, which determines the temperature excursion from heating by the pump beam, and the temperature dependence of the optical reflectivity, which determines the change in the intensity of the reflected probe beam created by the temperature excursion.

There have been numerous qualitative measurements of the thermoreflectance coefficient,  $dR/dT$ , of metallic elements [8–11], however only a few studies report quantitative values at isolated optical wavelengths [12–15]. Furthermore, it is prohibitively difficult to predict the thermoreflectance of a metal from other material properties because the temperature dependence of the optical constants [9] of metals depend on several factors: changes in the electron bands created by thermal expansion, changes in occupations of electron states near the Fermi level, and changes in the phonon population that alter electron scattering rates and perturb the electron energy bands through electron-phonon coupling. The  $dR/dT$  of thin metal films is further affected by elastic strains that develop as a result of thermal expansion mismatch between the film and substrate [9]. The lack of quantitative values for  $dR/dT$  as a function of wavelength is an unnecessary constraint in the design of pump/probe experiments.

In a standard TDTR or FDTR measurement the optical transducer is an opaque layer on the surface of the sample and the intensity fluctuations in the probe beam depend only on  $dR/dT$  of the transducer. Detailed knowledge of the temperature coefficients of the real and imaginary parts of the transducer's index of refraction,  $dn/dT$  and  $dk/dT$ , is not necessary. If the transducer in a pump/probe measurement is not optically opaque or is not on the surface of a multilayered sample, then the probe beam is no longer interrogating only the optical properties of the transducer. Therefore, intensity fluctuations of the reflected probe will depend on the temperature field throughout the sample region that is interrogated by the probe, and the values of  $dn/dT$  and  $dk/dT$  of all materials therein. Components of the measured signal that arise from temperature excursions away from the transducer are typically unwanted artifacts. While use of an opaque transducer on the sample surface prevents these artifacts, it is a severely limiting constraint that would preclude the use of ultrafast thermal analysis as a technique for studying many geometries of interest.

Two examples of such systems that partially motivate the present study are perovskite oxide interfaces and plasmonic nanomaterials. The well-ordered interfaces formed in oxide heterostructures make metallic perovskites enticing candidates as optical transducers for studies of interfacial thermal transport. However, the use of metallic perovskites as transducers is problematic because their small thermal conductivity produces a significant temperature drop in the transducer, thereby reducing experimental sensitivity to the thermal properties of the underlying sample. The thermal conductance of the transducer can be increased by making the transducer thinner, but this will result in the film becoming semi-transparent, and can produce unwanted signal artifacts from temperature excursions from the rest of the sample. Similar problems can arise in pump-probe studies of plasmonic nanostructures. The unique photothermal properties of plasmonic nanomaterials have motivated extensive research into how they exchange thermal energy with their surroundings [16]. But thermal analysis of pump-probe measurements that use plasmonic nanomaterials as the optical transducer are highly susceptible to the type of artifacts described above because the shape, strength, and optical frequency of the plasmonic resonance depends strongly on the material's surrounding dielectric environment [17]. Artifacts that result from non-opaque transducers can be minimized through careful experiment design. For example, the wavelengths of pump and probe beams can be chosen so that the artifact is minimized and the response of the transducer is maximized. However, this type of design necessitates quantitative values for  $dn/dT$  and  $dk/dT$  of the transducer as a function of optical wavelength; values that are not currently available in the literature.

The present work has two primary goals. The first goal is to provide values of  $dR/dT$  of fifteen high purity bulk metals at the wavelength generated by Yb: fiber laser oscillators (1.03  $\mu\text{m}$ ). The second goal of the present work is to provide values for  $dR/dT$  of thin metal films of Pt, Ta, Al, Au, SrRuO<sub>3</sub>, and LaNiO<sub>3</sub> across a wide wavelength range,  $0.4 < \lambda < 1.6 \mu\text{m}$ , using variable-angle spectroscopic ellipsometry. The temperature dependent ellipsometry results validate our experimental approach of using TDTR as a quantitative probe of temperature coefficients. The ellipsometry results provide values across a wide wavelength range for  $dn/dT$  and  $dk/dT$  of the thin film samples of Pt, Au, SrRuO<sub>3</sub>, and LaNiO<sub>3</sub>. The values of  $dn/dT$  and  $dk/dT$  reported for Au and Pt will assist in the analysis and design of heat transfer studies of plasmonic nanomaterial systems. Similarly, the values of  $dn/dT$  and  $dk/dT$  reported for SrRuO<sub>3</sub> and LaNiO<sub>3</sub> will assist in using ultrafast thermal analysis as a tool for probing interfacial properties of oxide heterostructures.

## 2. Experiment

The fifteen high-purity bulk metal samples are components of a commercially available "element standard" intended for calibration of x-ray emission intensity in analytical scanning electron microscopy. The Al metal film was deposited on a Si wafer and the Au, Pt, and Ta films were deposited on thermally oxidized Si wafers using dc magnetron sputtering. The

thickness of thermal oxide on the Si wafers was 500 nm. The Pt, Al, and Au films were deposited at room temperature. Ta was deposited on substrates held at  $\approx 700$  °C to form the  $\alpha$  (bcc) phase [18] of Ta.

Thin-films of SrRuO<sub>3</sub> and LaNiO<sub>3</sub> were grown via pulsed-laser-deposition using a KrF excimer laser in 100 and 250 mTorr of oxygen pressure from ceramic SrRuO<sub>3</sub> and LaNiO<sub>3</sub> targets. Laser ablation during the SrRuO<sub>3</sub> and LaNiO<sub>3</sub> growths was performed with a fluence of 0.68 J cm<sup>-2</sup> at a repetition rate of 14 and 5 Hz corresponding to a growth rate of 7 and 3 nm/min for the SrRuO<sub>3</sub> and LaNiO<sub>3</sub> films. The SrRuO<sub>3</sub> film was grown on a SrTiO<sub>3</sub> (001) substrate and the LaNiO<sub>3</sub> film was grown on a LaAlO<sub>3</sub> (001) substrate held at temperatures of 640 and 600 °C, respectively. Both films were cooled to room temperature at 5 °C/min in 760 Torr oxygen. The SrRuO<sub>3</sub> and LaNiO<sub>3</sub> film thicknesses were determined to be 49 and 60 nm, respectively, by x-ray reflectivity (XRR). (LaNiO<sub>3</sub> and LaAlO<sub>3</sub> have comparable densities making XRR difficult on a LaNiO<sub>3</sub>/LaAlO<sub>3</sub> sample. Therefore a SrTiO<sub>3</sub> (001) substrate was placed next to the LaAlO<sub>3</sub> substrate during growth and XRR was performed on this sample.)

We use TDTR to measure  $dR/dT$  of the bulk and thin-film samples at 1.03  $\mu\text{m}$  using a Yb: fiber laser that produces  $<200$  fs pulses at a 100 MHz repetition rate. A schematic is shown in Fig. 1. In TDTR, a train of laser pulses is split into pump and probe beams. The pump beam is modulated with a 50% duty cycle at 10 MHz by an electro-optical modulator. The probe beam is mechanically chopped with a 50% duty cycle at 200 Hz. A mechanical delay stage advances the arrival of the pump optical pulses relative to the probe optical pulses. A  $20\times$  objective lens with 70% transmission at 1.03  $\mu\text{m}$  focuses both pump and probe beams on the sample with  $1/e^2$  radius spot size of  $\omega_0 = 3.8$   $\mu\text{m}$ . Pump and probe powers are measured by a calibrated germanium photodetector prior to the objective lens. Typical values for the pump and probe beams are 16 and 8 mW, respectively.

The reflected probe beam is focused on an InGaAs photodiode with a 30 cm focal length lens. The output of the photodiode is sent through a preamplifier with a voltage gain of 5 and then measured by an rf lock-in amplifier synchronized to the modulation frequency of the pump beam (10 MHz). The rf lock-in amplifier incorporates a square wave mixer that is sensitive to unwanted odd harmonics of 10 MHz present in the probe signal (the signal includes components at odd multiples of 10 MHz because the pump beam is modulated with a square wave). Therefore, we add a low pass filter with a cutoff frequency of 21.4 MHz to attenuate higher odd harmonics. The output of the rf lock-in is measured by two computer-based audio frequency lock-in amplifiers that are synchronized to the 200 Hz frequency of the mechanical chopper in the path of the probe beam. This removes background signals created by coherent rf pickup.

To prevent diffusely scattered pump light from reaching the InGaAs detector, we use sharp edged optical filters to spectrally separate the pump and probe beams, making our TDTR setup a two-tint pump-probe experiment [19]. The Yb:doped fiber laser we use in our TDTR measurements has a broad spectral output centered at 1.03  $\mu\text{m}$  with a spectral width of 0.03  $\mu\text{m}$ . We use a 1.064  $\mu\text{m}$  ultra-steep long-pass filter to split the laser output into the pump and probe beams. Our setup contains a polarizing beam splitter prior to the long-pass filter; therefore the beam incident on the long-pass filter is S-polarized. By setting the angle of incidence to 35°, the 50% transmission wavelength for S-polarized light is shifted to 1.03  $\mu\text{m}$ . We use the transmitted spectral portion of the beam as the probe and the reflected portion as the pump. To block diffusely scattered pump light from reaching the InGaAs detector after being reflected from the sample we place two Semrock 1.064  $\mu\text{m}$  dichroic beamsplitters immediately prior to the InGaAs detector. By setting the angles of incidence to  $\sim 55$  and  $56^\circ$  the 50% transmission wavelength of S- and P- polarized light is shifted near 1.03  $\mu\text{m}$ . Two beam splitters are required to fully block the pump beam because the 50%

transmission wavelengths for S- and P- polarized light differ by  $\sim 4$  nm for a single angle of incidence.

We measure the temperature dependence of the optical constants of Au, Al, Ta, Pt, SrRuO<sub>3</sub> and LaNiO<sub>3</sub> thin-films as a function of wavelength by collecting variable angle spectroscopic ellipsometry (VASE) data at  $T = 25$  °C and  $T = 157$  °C. (For Ta, we used an upper temperature of 96 °C to avoid possible problems created by oxygen incorporation in the Ta lattice.) We used a commercial Woolam ellipsometer to collect spectra in  $(\Delta, \Psi)$  at angles of incidence of 60 and 80° between 0.4 and 1.6  $\mu\text{m}$ . The standard optical stage of the Woolam ellipsometer was replaced with a home-built optical stage equipped with a small thermoelectric heater to enable the sample temperature to be raised. To obtain the optical constants of the four elemental metal films at the two temperatures from the raw ellipsometry data, we created Drude-Lorentz oscillator models for each set of ellipsometric data.

The Au, Al, Ta, and Pt films are optically thick, i.e., transmission is negligible. The 49 nm SrRuO<sub>3</sub> and 60 nm LaNiO<sub>3</sub> films are semitransparent and the index of refraction of the substrates impacts the ellipsometric spectra. Therefore, to obtain optical constants of SrRuO<sub>3</sub> and LaNiO<sub>3</sub> at the two temperatures, the ellipsometric spectra were analyzed with a thin-film model with parameters for film thickness, film index of refraction and extinction coefficient, and substrate index of refraction. The index of refraction as a function of wavelength of SrTiO<sub>3</sub> and LaAlO<sub>3</sub> substrates was measured separately and the SrRuO<sub>3</sub> and LaAlO<sub>3</sub> film thicknesses were determined using XRR. (Accounting for changes in the thickness due to thermal expansion caused negligible changes in analysis).

The free parameters of all models (Drude-Lorentz oscillator models for the elemental metals and thin-film models for the perovskite metals) were determined by fitting to the experimental data using regression analysis. We could not obtain a good fit to the ellipsometric data of Au between 0.4 and 0.8  $\mu\text{m}$  with a Drude-Lorentz oscillator model. Therefore, in this spectral region, we calculate  $dR/dT$  from the pseudo-optical constants derived directly from the ellipsometry spectra taken at the two temperatures. (Ellipsometric spectra were not collected between 1.34 and 1.42  $\mu\text{m}$  due to an absorption band in the optical fiber of the ellipsometer.)

To verify the accuracy of our ellipsometric measurements, we measured the index of refraction of a Si substrate with 3 nm of native oxide at 140 and 25 °C. Our measured values for Si of  $(1/n)(dn/dT)$  of 5.6, and  $5.2 \times 10^{-5} \text{ K}^{-1}$  at 1.3 and 1.5  $\mu\text{m}$  agree well with previously reported values [20] of 5.4 and  $5.1 \times 10^{-5} \text{ K}^{-1}$  at these two wavelengths.

### 3. Results and discussion

The root-mean-square (rms) voltage measured by the rf lock-in amplifier at the modulation frequency of 10 MHz is related to the change in temperature from pump beam heating,  $\Delta T(t)$ , by

$$V(t) = \frac{G}{\sqrt{2}} \frac{2V_0}{R} \frac{dR}{dT} \Delta T(t), \quad (1)$$

where  $G$  is the gain of the preamplifier,  $V_0$  is the average dc voltage read by the InGaAs detector, and  $R$  is the optical reflectivity of the metal. The factor of two accounts for the reduction in the output voltage of the InGaAs detector created by audio frequency chopping of the probe beam. The signal output of the rf-lock-in that is measured by the computer-based audio frequency lock-in is a square wave at 200 Hz (due to the mechanical chopping of the probe) with a peak-to-peak voltage of  $V(t) \times (10 \text{ Volt}/S)$ , where  $S$  is the sensitivity setting of the rf-lock-in amplifier. The computer-based audio frequency lock-in amplifier measures the amplitude of the 200 Hz harmonic component of this square wave output. Therefore, the

audio frequency lock-in measures a voltage that is a factor of  $(4/\pi) \times (5\text{Volt/S})$  higher than  $V(t)$ . We correct for this numeric factor in our data acquisition software.

The temperature rise of the metal surface,  $\Delta T(t)$ , is calculated using an analytical solution to the heat diffusion equation in cylindrical coordinates [1]. The temperature rise at the surface of the metal depends the average energy absorbed by the metal at 10 MHz,  $A_f = (2/\pi)(1-R)P_0$ , where  $P_0$  is the average power incident on the metal surface. The thermal conductivity and heat capacity of the bulk metals was taken from Ref [21]. We use four-point probe measurements of the in-plane electrical conductivity and the Wiedemann-Franz law to estimate the thermal conductivities of the thin metal films. The thermal conductivity of the Al, Ta, Au, Pt films are 120, 55, 200, 55  $\text{W m}^{-1} \text{K}^{-1}$ , respectively. In the case of the thin metal films, the temperature rise of the metal surfaces at a delay time of 300 ps is only weakly dependent on the thermal conductivity because 300 ps is longer than the time it takes the metal films to thermalize. To calculate the power absorbed, we use previously reported reflectance values [22, 23] for the bulk metals. For the thin-film samples we use the reflectance derived from the ellipsometry data at 1.03  $\mu\text{m}$ .

The in- and out-of-phase voltages measured by the rf lock-in for thin-film Al and bulk Ta and Ru as a function of delay time are shown in Fig. 1, along with the prediction of the right-side of Eq. (1). The rms voltages measured by the rf lock-in at 300 ps delay time for the fifteen metal standards and four thin metal films are shown in Fig. 2(a). The corresponding values of  $dR/dT$  calculated from Eq. (1) are shown in Fig. 2(b). Al, Ta, Re, and Ru have high values of thermorefectance at 1.03  $\mu\text{m}$ ,  $dR/dT > 6 \times 10^{-5} \text{K}^{-1}$ .

Uncertainties in the parameters required to derive  $\Delta T$  can cause significant uncertainties in the calculated value of  $dR/dT$ . For highly reflective metals, such as Al and Au, a small error in reflectance can cause large uncertainties since  $\Delta T \propto (1-R)$ . We estimate the uncertainty in our measured values of  $R$  to be  $\sim 1\%$  based on the differences in our TDTR ratio makes it difficult to accurately set the phase of the reference channel of the rf lock-in and even small spurious electrical signals can cause a significant error.

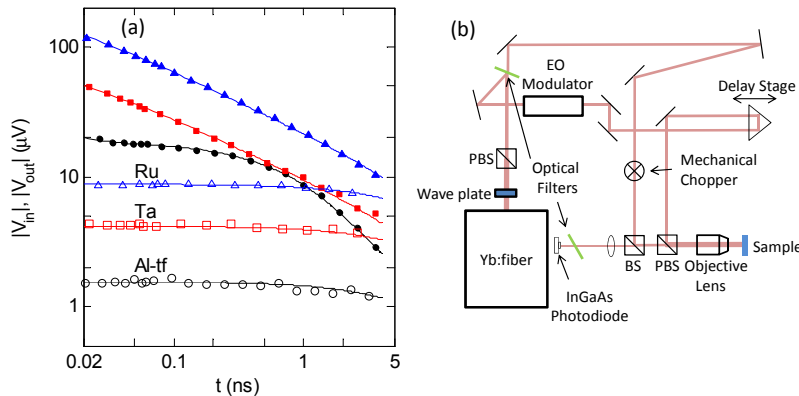


Fig. 1. (a) Thermorefectance data as function of pump-probe delay time for a 80 nm sputtered thin-film of Al on Si (circles, labeled Al-tf), high purity bulk Ta (squares) and high purity bulk Ru (triangles). The in-phase or real part of  $V(t)$  is plotted as solid symbols and the out-of-phase or imaginary part of  $V(t)$  is plotted as open symbols. The lines are the real and imaginary parts predicted by the right hand side of Eq. (1) with  $dR/dT = -6.4 \times 10^{-5} \text{K}^{-1}$ ,  $dR/dT = -1.4 \times 10^{-4} \text{K}^{-1}$ , and  $dR/dT = 1.5 \times 10^{-4} \text{K}^{-1}$  for Al, Ta, and Ru, respectively. (b) Schematic of the optical layout for the TDTR measurements.

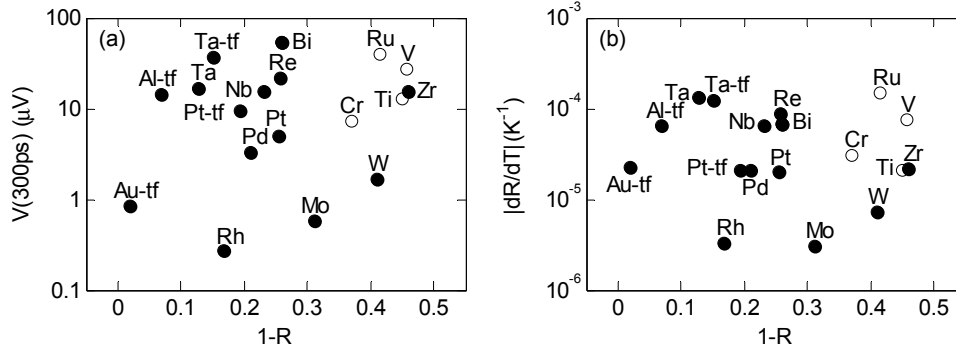


Fig. 2. (a) Absolute value of the signal detected by the rf lock-in in the TDTR measurements at a time-delay between pump and probe of  $t = 300$  ps. The laser source is an Yb: fiber oscillator operating at a wavelength of  $1.03 \mu\text{m}$ . The average pump and probe powers are 16 and 8 mW respectively. (b) Absolute value of the thermoreflectance based on the signal strength plotted in panel (a) in combination with Eq. (1). Filled circles denote negative values of  $dR/dT$  and open circles denote positive values of  $dR/dT$ . Thin-film samples have the tag “-tf” added to the name of the element.

If the reflectance is not too close to 1, and the signal not too small, the dominant source of error is the uncertainty in the  $1/e^2$  radius of the focused laser spot  $\omega_0$  because  $\Delta T \propto 1/\omega_0^2$ . We characterize this parameter in two ways. First, we analyze the in-phase voltage measured by the rf lock-in at 80 ps delay time as a function of the offset distance between focused pump and probe beams on the thin Ta film sample. The in-phase voltage at short delay times is proportional to the convolution of the intensity profile of the pump and probe. Since the pump and probe beams have approximately equal spot sizes, the in-phase signal simplifies to  $V_{in} \propto \exp(-x^2/\omega_0^2)$ , where  $x$  is the linear offset between the center of the pump and probe beams. Our second method for characterizing the laser beam radii is to analyze optical images of reflections of the focused pump and probe beams taken by a CCD camera. The spatial correlation and microscopic imaging measurements yield comparable values of  $3.8$  and  $4 \mu\text{m}$ , respectively. We use the spatial correlation value in our analysis and estimate the uncertainty in the spot size as twice the difference in these two measurement techniques. Using an uncertainty of 10% in the value of  $\omega_0$ , 1% in the values of  $R$  used to calculate the temperature rise, and  $0.2 \mu\text{V}$  in the measured in-phase rms voltage, then the uncertainties in  $dR/dT$  will be 80, 60, 35, and 25% for Rh, Au, Mo, and Al, respectively. These metals have large uncertainties because they have small values of either  $dR/dT$  or  $(1-R)$ . All other metals have an uncertainty in  $dR/dT$  of  $\sim 20\%$  arising primarily from the uncertainty in  $\omega_0$ . The optical constants of the  $\text{SrRuO}_3$ , and  $\text{LaNiO}_3$  metal films measured by spectroscopic ellipsometry are shown in Fig. 3. (We do not report the optical constants of the elemental metal films as these values have been reported previously [22].) The temperature coefficients of  $n$  and  $k$  of Pt, Au,  $\text{SrRuO}_3$ , and  $\text{LaNiO}_3$  as a function of wavelength are shown in Fig. 4(a) and Fig. 4(b). The temperature coefficients of  $n$  and  $k$  for Al and Ta are not reported because the values derived from the ellipsometric spectra are sensitive to the optical thickness of the native oxide layer, a value we do not know precisely.

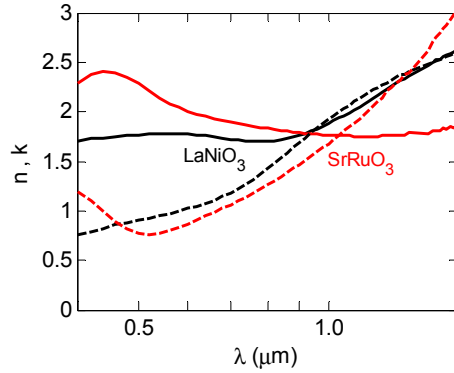


Fig. 3. Room temperature real (solid lines) and imaginary (dashed lines) part of the index of refraction of SrRuO<sub>3</sub> and LaNiO<sub>3</sub> metallic oxide films as function of wavelength between 0.4 and 1.6 μm.

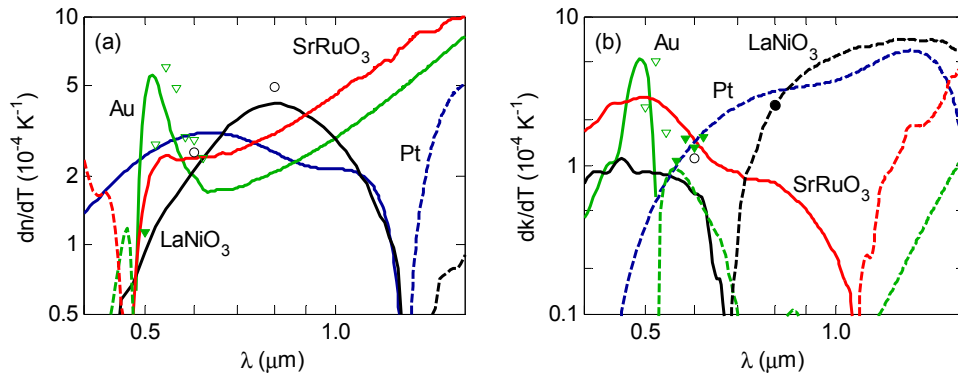


Fig. 4. Temperature coefficient of the real (a) and imaginary (b) part of the index of refraction for Pt, Au, SrRuO<sub>3</sub> and LaNiO<sub>3</sub> metal films. The triangles are data taken from Ref. [14], and the circles are data taken from Ref. [22]. Filled symbols denote negative values and open symbols denote positive values.

The absorbance,  $(1-R)$ , of the Pt, Ta, Al, Au, SrRuO<sub>3</sub>, and LaNiO<sub>3</sub> metal films measured by spectroscopic ellipsometry is shown in Figs. 5(a) and 5(b). The thermorefectance as a function of wavelength of the Pt, Ta, Al, and Au films is shown in Fig. 5(b), and the thermorefectance as a function of wavelength of SrRuO<sub>3</sub> and LaNiO<sub>3</sub> is shown in Fig. 5(c). While the metallic oxide films we studied are not optically thick, Fig. 5 shows the values of  $(1-R)$  and  $dR/dT$  calculated for optically thick films based on the assumption that the complex index of refraction of SrRuO<sub>3</sub> and LaNiO<sub>3</sub> is independent of film thickness.

Figure 5(b) includes TDTR measured values of  $dR/dT$  of the four elemental metal films at 0.785 μm and 1.03 μm for comparison. The agreement between the two techniques validates the ability of TDTR to quantitatively probe temperature coefficients. The absorbance and  $dR/dT$  of the SrRuO<sub>3</sub>/SrTiO<sub>3</sub> and LaNiO<sub>3</sub>/LaNiO<sub>3</sub> samples depend on the film thicknesses of 49 and 60 nm as well as the substrate index of refraction and are not intrinsic values of the materials SrRuO<sub>3</sub> and LaNiO<sub>3</sub>. Therefore, we do not include TDTR measurements of these samples for comparison in Fig. 5. The TDTR apparatus we use to measure  $dR/dT$  at 0.785 μm has been described previously [12,19] and is nearly identical to that described above, but uses a Ti:sapphire laser with a fundamental wavelength of 0.785 μm.

As expected, Au, Al, and Ta show large values of the thermorefectance at wavelengths nearby in energy to band resonances at  $\approx 0.5$ ,  $0.6$ , and  $0.8 \mu\text{m}$ , respectively. The most commonly used optical transducer in TDTR experiments, Al, has a high thermorefectance across most of the infrared ( $0.8 < \lambda < 1.6 \mu\text{m}$ ) but is a poor choice as a transducer for  $\lambda < 0.7 \mu\text{m}$ . The metallic oxides SrRuO<sub>3</sub> and LaNiO<sub>3</sub> both have high values of  $dR/dT$  across the infrared spectrum and are suitable transducers for TDTR and FDTR experiments in this spectral region.

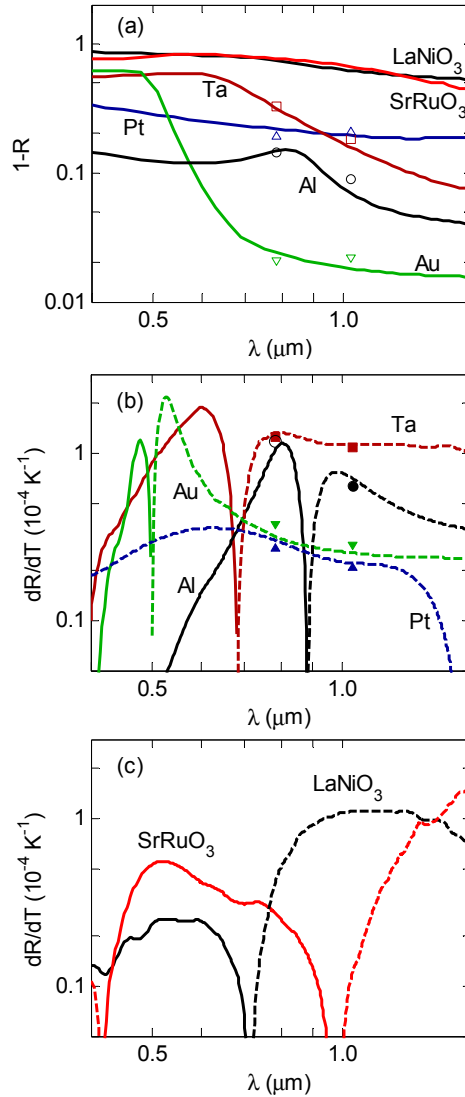


Fig. 5. Absorbance (a) and thermorefectance measured by spectroscopic ellipsometry for Pt, Ta, Al, and Au metal films (b) and SrRuO<sub>3</sub> and LaNiO<sub>3</sub> metallic oxide films (c). Solid lines indicate positive values and dashed lines indicate negative values. The circles, squares, up-triangles, and down-triangles represent the TDTR measured absorbance and thermorefectance values for the Pt, Ta, Al, and Au films at 0.785 and 1.03  $\mu\text{m}$ . Filled symbols denote negative thermorefectance values and open symbols denote positive values. The data point for the TDTR measured thermorefectance of Al at 0.785  $\mu\text{m}$  is partially obscured by the Ta data point.

The optical properties of a metal that determine its merit as a thermometer depend on the source of noise in the measurement. Equation (1) predicts the signal for a fixed temperature change will be proportional to the average probe beam power  $A_p$  and  $dR/dT$  because  $V_0/R \propto A_p$ . If the dominant source of noise is the electronics (such as Johnson noise from the detector) then noise is independent of probe power and the figure-of-merit as a thermometer is  $dR/dT$ . However, if the dominant source of noise is high frequency fluctuations in the intensity of the probe beam, then the noise scales with  $RA_p$  (the probe power incident on the detector) and the figure-of-merit as a thermometer is  $(1/R)(dR/dT)$ . By this metric, Ta, Re, Ru, and V are the best thermometers at 1.03  $\mu\text{m}$  with  $(1/R)(dR/dT) > 10^{-4} \text{ K}^{-1}$ . Ta between 0.52 and 0.65  $\mu\text{m}$ , SrRuO<sub>3</sub> between 0.49 and 0.59  $\mu\text{m}$  and LaNiO<sub>3</sub> between 0.85 and 1.3  $\mu\text{m}$  are all exceptionally sensitive thermometers with  $(1/R)(dR/dT) > 2.5 \times 10^{-4} \text{ K}^{-1}$ . In many experiments, however, the additional sensitivity a transducer gains from a small reflectance will be negated by constraints imposed by large steady-state heating that can result from a large value of  $(1-R)$ .

Our results are in good agreement with prior investigations. We observe a similar wavelength dependence for  $dR/dT$  of Ta, Al, and Au as previous qualitative thermoreflectance measurements of bulk crystals [9–11, 13]. The magnitude of  $dn/dT$  and  $dk/dT$  measured for the Au film (Fig. 4) between 460 and 640 nm is in agreement with values reported by Ref [14]. for single crystal Au at 10 and 310 °C, although Ref. 14 values predict a change in the sign of  $dR/dT$  at 0.54  $\mu\text{m}$  as opposed to the 0.50  $\mu\text{m}$  crossover we observe. A change in sign of  $dR/dT$  at 0.50  $\mu\text{m}$  is consistent with other thermo-reflectance investigations of Au [9, 11, 13]. Our measurements of the optical constant temperature coefficients of LaNiO<sub>3</sub> are in reasonable agreement with a previous ellipsometry study [24] of PLD-grown optically-thick LaNiO<sub>3</sub> on a SrTiO<sub>3</sub> substrate at temperatures between 118 and 650 °C.

We expect the temperature dependence of the reflectance of Au and Al in the near infrared to be described well by a free electron Drude model that neglects inter-band transitions. The Drude model predicts that the temperature dependence of the electron scattering rate will be the only significant contribution to the thermoreflectance. While the Drude model underpredicts the absorbance of Au and Al in the near-infrared because of the anomalous skin-effect [25], the Drude model should provide an accurate description of the thermoreflectance because the temperature dependence of electron scattering rates at these frequencies will be dominated by changes in the phonon-population and therefore well described by the temperature dependence of the dc electrical conductivity. The Drude model predicts a thermoreflectance for Al and Au of  $-4.7 \times 10^{-5} \text{ K}^{-1}$ , and  $-1.9 \times 10^{-5} \text{ K}^{-1}$ , within 25% of our ellipsometry measurements for Al and Au at 1.6  $\mu\text{m}$  of  $-3.5 \times 10^{-5} \text{ K}^{-1}$  and  $-2.3 \times 10^{-5} \text{ K}^{-1}$ .

#### 4. Conclusion

We used TDTR to measure the values of  $dR/dT$  for fifteen bulk metallic elements at 1.03  $\mu\text{m}$  and used spectroscopic ellipsometry to measure  $dR/dT$  of thin Pt, Ta, Al, Au, SrRuO<sub>3</sub>, and LaNiO<sub>3</sub> films between the wavelengths of 0.4 and 1.6  $\mu\text{m}$ . This will aid experimentalists in the design of experiments for characterizing thermal properties on nanoscale length scales.

#### Acknowledgments

This work was supported by the U.S. Department of Energy Office of Basic Energy Sciences, under Award Grant No. DE-FG02-07ER46459 and was carried out in the Laser and Spectroscopy Laboratory of the Materials Research Laboratory at the University of Illinois Urbana Champaign. R. B. Wilson thanks the Department of Defense for the NDSEG fellowship that supported him during this work.